Depositional Flux of Cosmogenic ^{10}Be in Southern India

A Thesis

submitted to

Indian Institute of Science Education and Research Pune in partial fulfilment of the requirements for the BS-MS Dual Degree Program

by

Muhammed Mehafus Thannani

Indian Institute of Science Education and Research Pune

Dr. Homi Bhabha Road,

Pashan, Pune 411008, INDIA.

March, 2025

Supervisor: Dr. Amzad Hussain Laskar

Certificate

This is to certify that this dissertation entitled **'Depositional Flux of ^{10}Be in Southern India'** towards the partial fulfilment of the BS-MS dual degree programme at the Indian Institute of Science Education and Research, Pune represents study/work carried out by Muhammed Mehafus Thannani at Physical Research Laboratory, Ahmedabad under the supervision of Dr. Amzad Hussain Laskar, Associate Professor, Geosciences Division, during the academic year 2024-2025.

Dr. Amzad Hussain Laskar
Associate Professor
Geosciences Division
PRL, Ahmedabad

Committee:
Dr. Amzad Hussain Laskar
Dr. Gyana Ranjan Tripathy

This thesis is dedicated to My Parents

DECLARATION

I hereby declare that the matter embodied in the report entitled "**Depositional Flux of ^{10}Be in Southern India**" are the results of the work carried out by me at the Geosciences Division, Physical Research Laboratory, Ahmedabad under the supervision of Dr. Amzad Hussain Laskar, and the same has not been submitted elsewhere for any other degree.

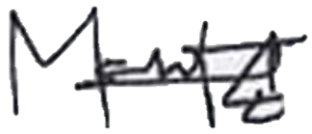

Muhammed Mehafus Thannani

20201076

BS-MS

IISER Pune

Table of Contents

List of Figures

List of Tables

List of Equations

ABSTRACT

The sun and the other exploding stars in our galaxy are a regular source of cosmic rays. These rays contain particles- mostly protons (~90%), alpha particles and small fraction of bigger nuclei. These particles, which are of both galactic and solar origin, have high energy such that they are able to penetrate the heliosphere (in case of the galactic cosmic rays) and the geomagnetic field of the earth, and then reach earth's atmosphere, where they generate a cascade of secondary particles. These secondary cosmic rays are able to knock out few nucleons from the nuclei of atmospheric gases, leaving behind a lighter nucleus. These newly formed nuclides are the cosmogenic nuclides. The isotope ^{10}Be is one such radionuclide formed by this spallation process and it has a half -life of $1.39*10^6$ years.

The ^{10}Be produced in the atmosphere, named meteoric ^{10}Be, binds to aerosols and reaches the surface of Earth through both wet and dry deposition., where they adsorb strongly onto to soil, sediment, ice pits, speleothems etc. The meteoric ^{10}Be serves as a valuable geochemical tracer for plenty of earth science applications across various natural environments, like assessing erosion, surface stability, quantifying denudation rates etc. The prerequisite for such applications is the depositional fluxes of ^{10}Be to the diverse geographical settings. Except in regions with low rainfall, the wet deposition exceeds dry deposition. Though some studies have suggested that its flux correlates with precipitation, others have shown the dilution of ^{10}Be with higher levels of precipitation. The present work tries to investigate the existence of any such relation between the flux of meteoric ^{10}Be and precipitation along a rainfall gradient region in India. The ^{10}Be concentration in soil increases with annual rainfall in places receiving <1500 mm y^{-1} and decreases with rainfall in regions having > 1500 mm y^{-1} annual rainfall. The flux values in these regions also shows a similar pattern of deposition and its value ranges from $0.32*10^6$ to $3.13*10^6$ atoms/cm^2/year.

ACKNOWLEDGEMENT

I would like to convey my deepest gratitude to Dr. Amzad Hussain Laskar, for his unwavering mentorship, support and guidance. I am very grateful for receiving such a wonderful opportunity to do my project in an institute like PRL with a rich legacy. I will always be indebted to him.

I wish to express my gratitude to Dr. Gyana Ranjan Tripathy for his valuable input and suggestion, which shaped the course of the project.

This work could not have been completed without the help of Mr. Ankur J Dhabi, who taught me the chemical procedure and was always with me from beginning to the end.

I sincerely thank Mr. Bankim Pandya for accompanying me during my field trip and helping me with sample collection.

My heartfelt gratitude also goes to Dr. A.K Sudheer who helped me with the analysis of stable isotope and helped me throughout the project.

I will always be grateful to Mr. A. Shivam, Mr. Mahesh and Ms. Vruthi, who helped with the analytical instruments.

I sincerely thank all the members of the Radiocarbon Laboratory at PRL. The time I spent with Rahul, Ranjan, Aishwarya, Dr. Sanchitha and Dr. Milan was memorable and I had the opportunity to learn a lot from them.

I am always indebted to my professors at IISER who taught me valuable lessons in Earth sciences and to the PhD students under them, who have always helped me.

Finally, I thank my family and all my friends for their love and support.

1.INTRODUCTION

In the year 1912, the Austrian physicist Victor Hess made a landmark discovery which had opened the doors to a new world of matter and also of science. In his balloon flight experiments, he concluded that the rise in atmospheric ionization with altitude is caused by radiation originating from above and suggested that this radiation has an extraterrestrial source. Millikan named these radiation as ‘cosmic rays’ since they were thought to be gamma rays, which was later found to be incorrect. Since then, several advancements have been made in the study of cosmic rays in ionisation chambers, photographic emulsions and then later in accelerators, which paved the way for particle physics.

The cosmic rays include mostly protons (~90%), alpha particles and some heavier nuclei (Simpson,1983). These are highly energetic particles, with their energies ranging from few MeV to ~ 10^{20} eV. The important question now is from where does these particles come from. Based on their source of origin, they are commonly divided into two types; galactic cosmic rays (GCR) and solar cosmic rays (SCR). Galactic cosmic rays originate beyond the solar system, but within the same galaxy. They have very high energy (from hundreds of MeV to >1 GeV) and their primary sources are believed to be the shocks produced during astrophysical phenomena like supernovae explosions, gamma-ray bursts and pulsars (Baade and Zwicky, 1934; Grieder 2001). With these high energies, they traverse the interstellar medium and finally reaches the solar system and subsequently into the earth.

The other category of cosmic rays are the solar cosmic rays which emanate from our sun. They are also known as solar energetic particles and They are primarily linked to coronal mass ejections and solar flares. They have less energy compared to the GCRs (< 1GeV; typically 1-100 MeV). Both these cosmic rays are continuously being impinged onto the earth.

The kinetic energy of a cosmic ray particle far exceeds the binding energy of nucleons.. Upon entering the earth’s atmosphere, these highly energetic particles lead to nuclear disintegrations of atoms in the atmosphere, eventually resulting in the formation

secondary cosmic rays, consisting of neutrons, protons, mesons etc. They then proceed independently, each producing its own cascade. (Figure 1.1). These secondary particles are of low energy (10 – 100 MeV) such that they are capable of knocking out few nucleons from nuclei of atmospheric gases, so that most of target is left intact; without the complete disintegration of the nuclei and leaving behind a lighter nucleus– spallation (Lal et al., 1958). These spallation reactions result in the formation of isotopes of atoms and most of them are radioactive, with varying half-lives. Hence these nuclides are collectively known as cosmogenic radionuclides.

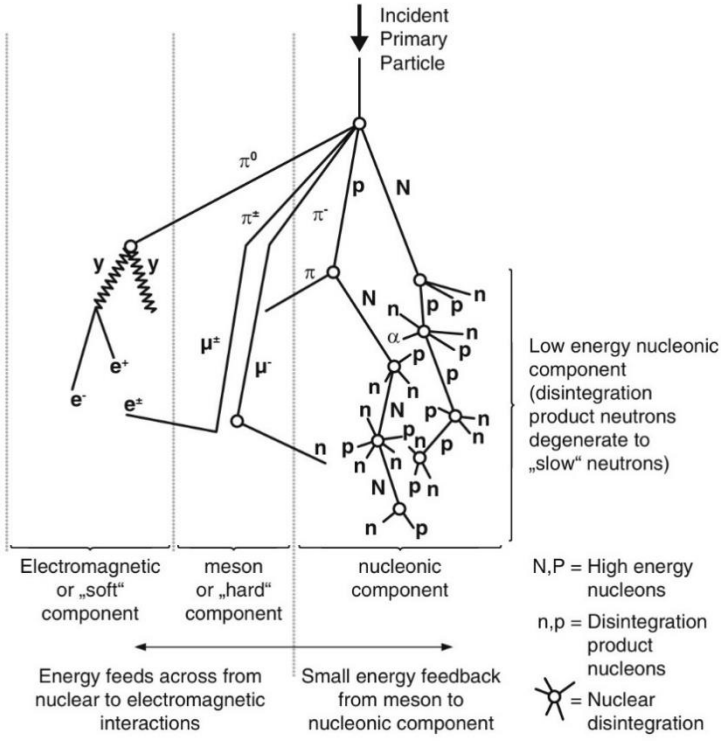

Figure 1.1: Nuclear cascade producing a shower of particles. The analogy given is that of nucleons acting as billiard balls. The cascade comprises nucleonic, mesonic, and electromagnetic components, with the nucleonic component being the most crucial for cosmogenic radionuclide production in the atmosphere, while mesons play a significant role deeper within the Earth's crust (Beer et al., 2012).

A myriad of such nuclides are produced by these cosmic ray particles. Some of them are listed in Table 1

Sl. No.	Cosmogenic Isotope	Major target elements	Half-life (in years)
1	^{3}He	All major elements	Stable
2	^{22}Ne	Mg, Al, Si	Stable
3	^{14}C	N	(5730 ± 40)
4	^{41}Ca	Fe, Ti	(104 ± 4) * 10^{3}
5	^{36}Cl	K, Ca, Cl	(301 ± 2) * 10^{3}
6	^{26}Al	Si	(708 ± 17) *10^{3}
7	^{10}Be	O, Si	(1.39 ± 0.01) *10^{6}
8	^{53}Mn	Fe, Mn	(3.7 ± 0.4) * 10^{6}

Table 1: Major cosmogenic radionuclides both stable and unstable, arranged in the increasing order of their half-lives (Dunai, 2010)

1.1 Latitudinal variation in Production

The flux of cosmic rays reaching Earth is not uniformly distributed in all directions. Their entry is influenced by variations in solar activity and the intensity of the geomagnetic field (Lal and Peters, 1967). Hence, the production of these radionuclides are modulated by these two factors Lower solar activity results in a weaker solar magnetic field carried by the solar wind, reducing the effectiveness of solar magnetic shielding. This results in greater GCRs reaching the Earth. It is also noteworthy to mention that at during periods of enhanced solar activity, even though the entry of GCRs are less, the Sun emits large amount of SCR. But their contribution to radionuclide production is very less since their energy is much less than GCRs. The contribution of these 'solar proton events' to ^{10}Be production accounts for only 1–2% of the total average ^{10}Be production rate (Usoskin et al., 2006)

The geomagnetic field of the earth also exhibit a similar shielding effect. It determines the cut-off rigidity, the minimum rigidity (rigidity - charged particle's sensitivity to the magnetic field and is defined as the ratio of its momentum to its charge) a charged particle must possess to penetrate the upper atmosphere and interact with atmospheric nuclei. Since the geomagnetic field is basically a dipole, this cut-off energy has a latitudinal dependence.

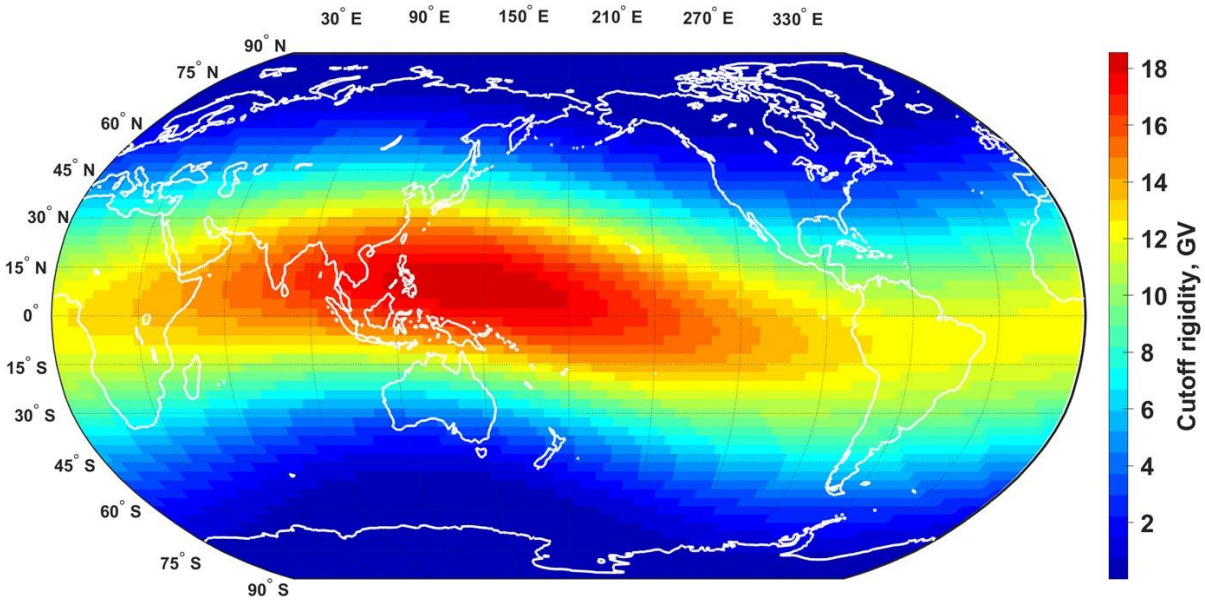

Figure 1.2: Vertical cut-off rigidity map for the 1992 epoch. (the cut-off rigidity is calculated using the Störmer formula: Cut-off rigidity, $P_c = 7.6 \,.\, M \left(\frac{R_0}{R}\right)^2 . \frac{cos^4\lambda}{\left(1+\sqrt{1+\sin\eta.\sin\phi.cos^3\lambda}\right)^2}$, where M represents the geomagnetic dipole moment (in 10^{22} A/m^2), R_o and R is the radius of the earth and the distance from the dipole center, respectively. λ is the geomagnetic latitude while the angles η and φ are the angle of zenith and the angle of azimuth from the geomagnetic north, of the incoming particle, respectively. The map shown corresponds to η = 0.) (Golubenko,2023)

The cut-off rigidity is maximum at the equator while it is almost zero at the polar latitudes. As a result, there is greater shielding at the equator compared to the geomagnetic poles, which lead to greater production of these nuclides at the higher latitudes, and less at the equator (Masarik and Beer,1999,2009).

1.2 Altitudinal Variation in Production

The cascade of secondary particles continues to an extent where they cannot cause further atom spallation, which happens because of the loss of considerable amount of energy by the particle during successive reactions as it moves/ falls to lower atmosphere. Hence, fewer reactions take place at lower altitudes since the cosmic ray particles have lower energy at lower altitudes. Consequently, the production rate in the upper atmosphere is greater than at the lower levels of the atmosphere. This leads to greater production of ^{10}Be in the stratosphere (65%) compared to troposphere (Lal & Peters, 1967; Masarik & Beer, 1999, 2009). The residence time of ^{10}Be is estimated to be 1–2 years in the stratosphere, whereas in the troposphere, it lasts only a few weeks. (Kulan, 2007)

1.3 Production of ^{10}Be

One such radionuclide formed by the spallation process is beryllium-10 (^{10}Be). They are formed through the spallation of oxygen and nitrogen atoms in the atmosphere, as well as in terrestrial rocks and surfaces. The former is called 'meteoric ^{10}Be' while the latter is called '*in-situ* ^{10}Be'.

Formation of meteoric ^{10}Be:

^{14}N (n,3p2n) ^{10}Be ^{14}N (p,4p1n) ^{10}Be

^{16}O (n,4p3n) ^{10}Be ^{16}O (p,5p2n) ^{10}Be

Unlike the meteoric ^{10}Be, '*in-situ'* ^{10}Be is generated through the capture of negative muons, as neutron energy becomes too low to trigger further reactions by the time it reaches the surface. Also, the greater penetrating ability enables them to reach deeper depths and produce ^{10}Be, especially in quartz grains (Gosse and Phillips, 2001).

^{16}O (μ^-,3p3n) ^{10}Be ^{16}O (μ^-,αpn) ^{10}Be

^{10}Be is produced from by spallation reaction produces 96.4% of total ^{10}Be production while muons are only responsible for the remaining 3.6% (Dunai, 2010).

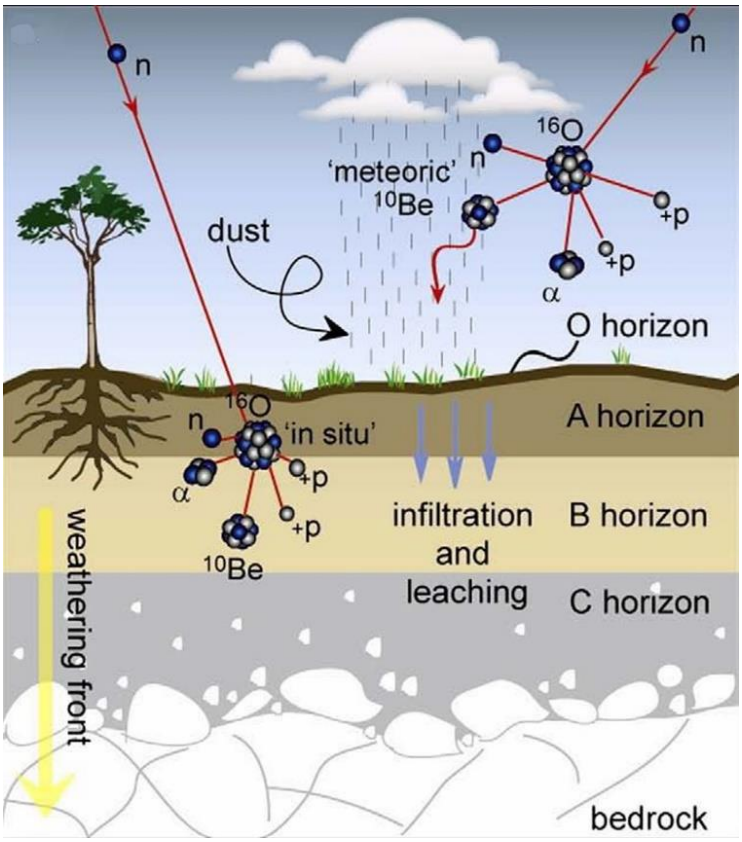

Figure 1.3: Meteoric and '*in-situ*' ^{10}Be (Willenbring and von Blanckenburg, 2010)

1.3.1 ^{10}Be and other cosmogenic isotope production models

The initial study of their production was done by the late Prof. Devendra Lal, Former director of Physical Research Laboratory (PRL) along with his mentor Prof. Bernard Peters. It was at a time when particle physics was coming into the picture. Despite his colleagues advising him to remain with the cosmic ray group, he went on to establish a geophysics group at the Tata Institute of Fundamental Research (TIFR) (Goswami and Macdougall,2021). The discovery of radioactive ^{14}C and cosmic-ray-produced tritium prompted them to explore other cosmic-ray-generated isotopes in nature for potential use in dating or tracing. They identified ^{7}Be and ^{10}Be as ideal candidates. They were able to separate out ^{7}Be from monsoon rainwater and ^{10}Be from deep sea sediments a year later (Goswami and Macdougall,2021). It is also noteworthy to mention that this work paved the way for isotope geochemistry in India.

Lal and Peters (1967) was the first to come up with an analytical model on nuclear disintegrations in the atmosphere. They empirically developed this model based on the star production rate, observed as multi-pronged tracks ("stars") created by cosmic ray interactions with nuclei in photographic emulsions. These emulsions were exposed for several years at varying altitudes and latitudes, capturing particle trajectories (Beer, 2010). The production rate was determined by multiplying the number of stars by the yield function, which represents the probability of a specific cosmogenic nuclide being produced.

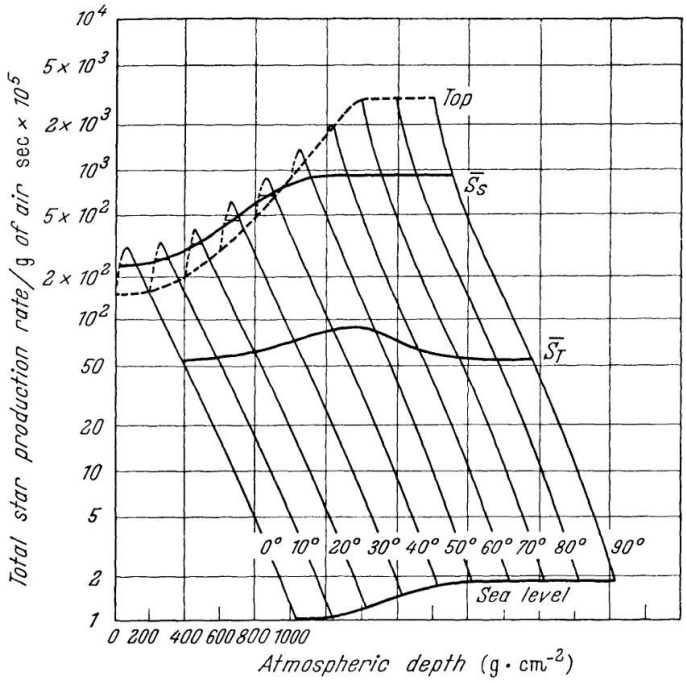

Figure 1.4: The star production rate, representing the number of nuclear disintegrations per gram of air per second, was plotted as a function of atmospheric pressure (depth) across different latitudes. By multiplying the ordinate scale with the yield factor 2.5 X 10^{-2}, the production rate of ^{10}Be can be calculated. (Lal and Peters, 1967).

With advancements in computational power, numerous models for ^{10}Be production have been developed worldwide. These models incorporate not only protons and neutrons but also alpha particles and heavy components of the cosmic ray flux in their calculations. The production rate can be calculated for different magnetic field intensities and for different solar modulation at different atmospheric depth and geomagnetic latitude.

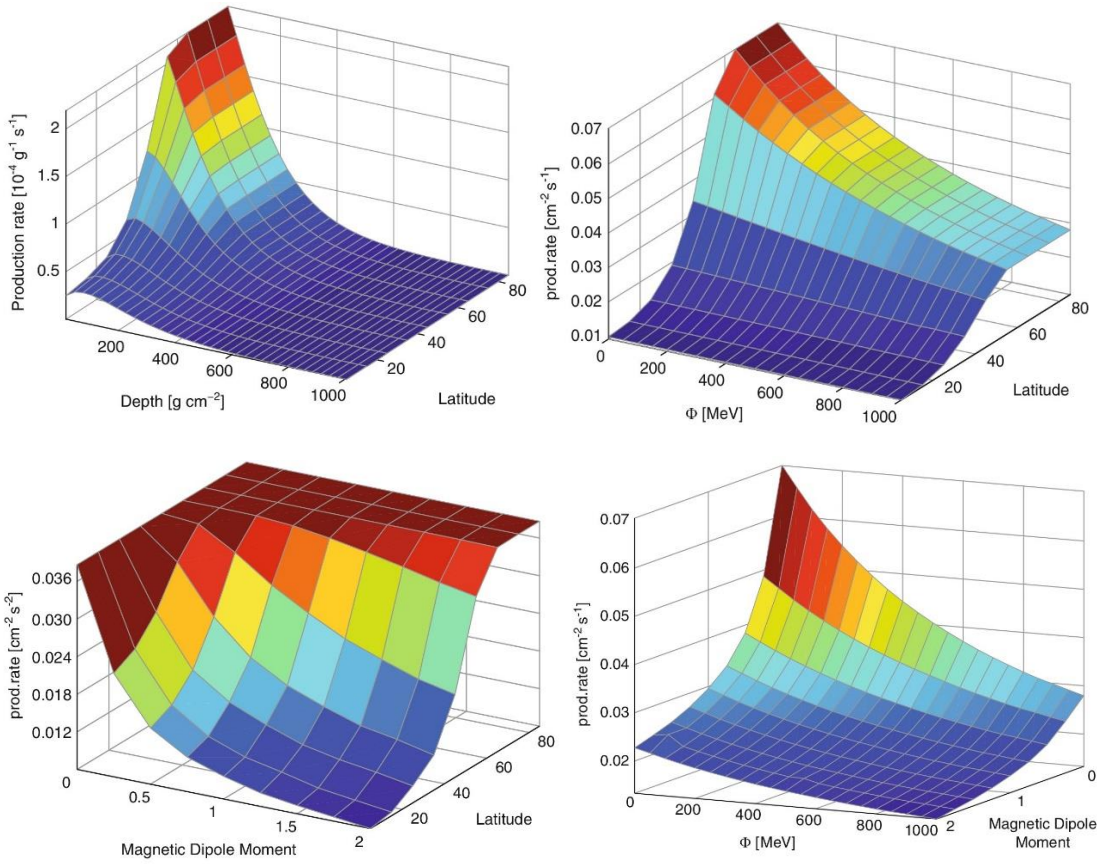

Figure 1.5: The ^{10}Be production rate, expressed in atoms per gram of air per second –
Top right: at different atmospheric depth and geomagnetic latitude, with the present magnetic field intensity and the solar modulation function fixed at 550 MeV (the intricate process of cosmic ray modulation by the Sun is simplified using a single parameter known as the solar modulation function, ϕ)
Top left: at different geomagnetic latitude and the solar modulation function, for the present-day geomagnetic field, integrated for the entire depth of the atmosphere.
Bottom right: at different relative geomagnetic dipole moment and the geomagnetic latitude, for fixed solar modulation of 550 MeV, determined by integrating across all atmospheric depths.
Bottom left: at varying geomagnetic dipole moment and level of solar modulation (Beer et al.,2010)

The combined influence of the increased cosmic ray flux at the poles, the greater atmospheric thickness at lower latitudes, and the lower pressure at the poles leads to a greater ^{10}Be production at midlatitudes (Willenbring and von Blanckenburg, 2010).

1.4 Deposition of ^{10}Be

Both meteoric ^{10}Be and in-situ ^{10}Be gradually accumulate in surficial deposits over time, with their concentration reflecting both the age and stability of the surface material. (Willenbring and von Blanckenburg, 2010).

The cosmic ray spectrum for the production of meteoric and *in-situ* ^{10}Be is different. As a result, the production of meteoric ^{10}Be is significantly higher than in-situ production, despite the greater elemental diversity in terrestrial matter. The meteoric flux is approximately 1 million atoms/cm^2/yr, whereas in-situ production ranges from about 2 to 20 atoms /g quartz/yr (McHargue and Damon, 1991; Willenbring and von Blanckenburg, 2010). The question of which variety of ^{10}Be should be used as a tracer depends on the application. The advantage of '*in-situ*' ^{10}Be over its meteoric counterpart is that it remains fixed at the location where it is produced. There are no uncertainities associated with it regarding its deposition and transport as they are always 'locked in'. The entire focus of the Earth surface process community turned towards *in-situ* nuclides after the pioneering work by Lal (Lal, 1991). The physical rules of production these *in-situ* nuclides were so well explained that the meteoric variety was sidelined for the past two decades (Willenbring and von Blanckenburg, 2010).

But application of ^{10}Be is limited due to the analytical and technical difficulties in its processing. The large amounts of pure, coarse-grained quartz needed for *in-situ* ^{10}Be measurement is not reliably available, in some of the sedimentary records, like lacustrine environments, offshore depo-centers etc (Willenbring and von Blanckenburg, 2010). Also, the chemical process of separating quartz, its digestion, purification etc and its analysis using highly expensive instruments make their processing cumbersome. There is no such dependency of meteoric ^{10}Be on any mineral or surface. It readily forms in the atmosphere through spallation and serves as an excellent geochemical tracer for evaluating erosion and surface stability across diverse natural setting. The prerequisite for such applications are the depositional fluxes of ^{10}Be to the diverse geographical settings.

After its production by gas-phase nuclear transformation in the atmosphere (Papastefanou, 2008), meteoric ^{10}Be gets adsorbed aerosol particles. It can also exist as a free aerosol of sub-micron size (Kulan,2007). Thus, its fate depends on the fate of the aerosols (Papastefanou, 2008). These aerosol particles carrying \(^{10}\)Be are deposited onto the Earth's surface through three mechanisms: wet deposition, dry deposition, and sedimentation (Laguionie et al., 2014; Schaar et al., 2024). Wet deposition or precipitation scavenging process is separated into two contributing components: rainout and washout processes (Bourcier et al, 2012; Rodhe and Grandell, 1972). In washout process the raindrops carry and incorporate particle as they fall during precipitation (below-cloud scavenging) while in rainout includes processes that occur within the cloud (in cloud- scavenging) by becoming a cloud-condensation nuclei, by attaching onto cloud particles by Brownian motion or by the transfer of aerosols to the droplets by the water vapour gradient (Junge,1963 cited in Rodhe and Grandell, 1972).

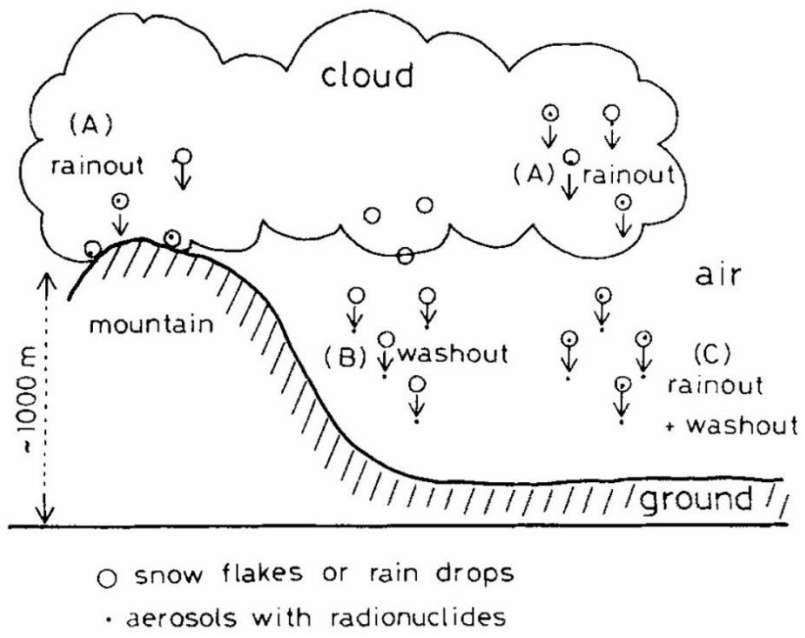

Figure 1.6: Rainout and washout process (Ishikawa et al., 1995)

Dry deposition happens in the absence of precipitation and it takes place through dry processes such as diffusion, impaction, or sedimentation (Schaar et al., 2024). It takes place when airborne particles attach to surfaces upon contact, including the Earth's surface or vegetation. Besides the physicochemical properties of the particles (e.g., larger

particle size) and deposition surfaces (e.g., surface friction), deposition also depends on micrometeorological factors such as local wind patterns and atmospheric conditions (Laguionie et al., 2014). Though it is a continuous process through time, it's contribution is only 10% of the total deposition (Heikkila et al., 2009). Wet deposition generally surpasses dry deposition, except in areas with low precipitation rates, such as the polar latitudes and coastal deserts of South Africa and South America (Schaar et al., 2024).

Kaste and Baskaran (2012) estimates the amount of ^{10}Be in rain and snow on the order of 10^4 atoms g^{-1}. They also hold the view that compared to latitude, precipitation has a stronger correlation to ^{10}Be flux. This assumption comes from the impact of another player- climate. For flux estimation, the stratosphere and troposphere are commonly assumed to be internally well mixed. Atmospheric mixing reduces variations in latitudinal production, causing the deposited ^{10}Be at a given latitude to represent the global mean production rate rather than the local production at that specific latitude. Although ^{10}Be production is higher in the stratosphere (about 10-50 times higher concentration compared to troposphere, (Jordan et al., 2003)), their transport and deposition is more controlled by the troposphere. The latitudinal patterns of large-scale atmospheric circulation in the troposphere strongly influences their flux, leading to greater deposition in mid-latitudes compared to poles and the tropics.

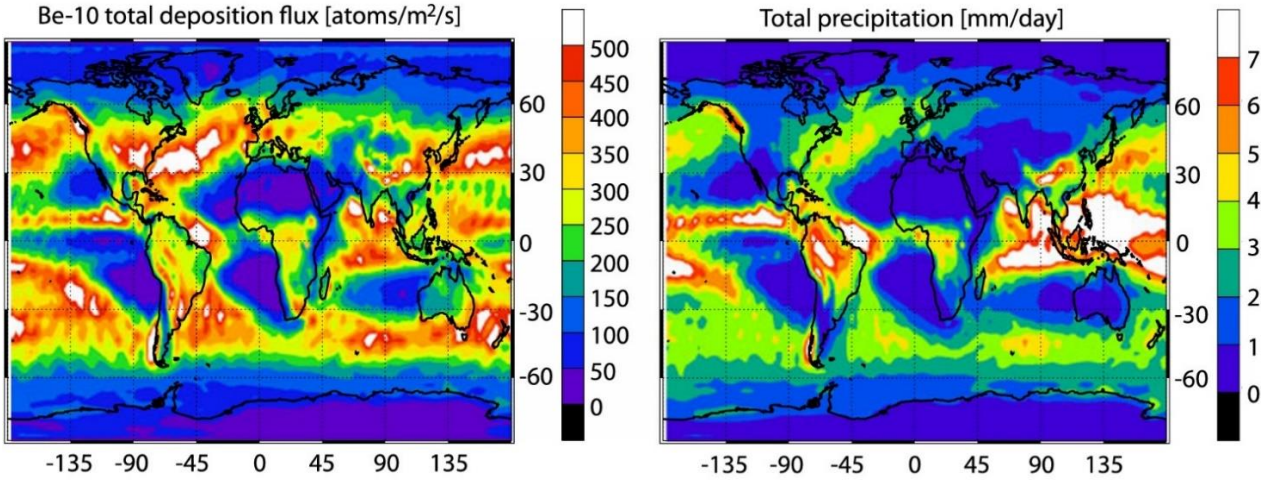

Figure 1.7: The depositional flux of ^{10}Be, averaged over the years 1986–1990, modelled using the ECHAM5-HAM general circulation model, along with the precipitation rate for the same period (Heikkila et al., 2013).

Figure 1.7 clearly shows that the deposition of ^{10}Be is higher in regions of high precipitation. Its deposition, as seen from the figure is high in the mid-latitudes, as these are the region where most of the stratosphere-troposphere exchange occurs. Several studies were done by people around the world wherein they tried to find out the annual ^{10}Be flux from precipitation collections. Graly et al., (2011) combined data from different latitudes and came to conclusion that the primary ^{10}Be flux strongly correlates to precipitation at mid and low latitudes. He also found that this holds true for both periodic comparison at a single site and when multiple sites within the same latitudinal bands are compared against each other.

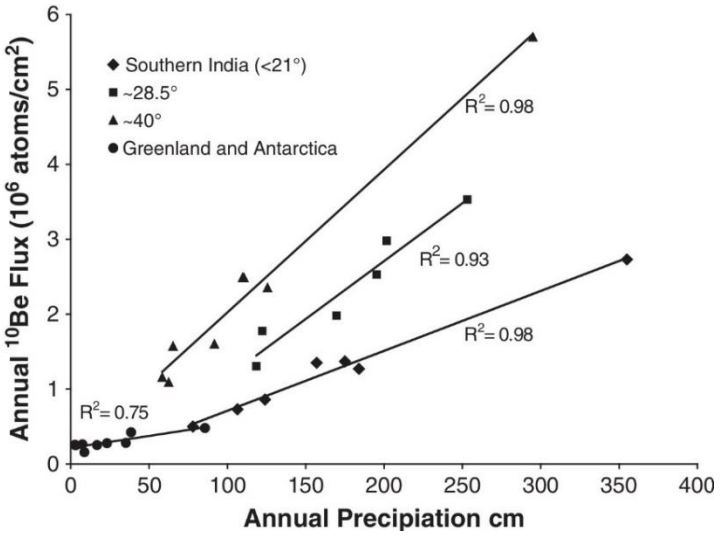

Figure 1.8: Strong precipitation control on ^{10}Be flux (Graly et al., 2011)

But these measurements of ^{10}Be in precipitation are 'short term' deliver rates. Over geomorphic timescales, well-constrained long-term meteoric ^{10}Be deposition rates are essential for its application as a chronometer or a tracer of Earth surface processes. The temporally averaged meteoric ^{10}Be fallout rate can be determined from minimally eroded, dated soils (Graly et al., 2011). Since most soils retain all deposited meteoric ^{10}Be within the soil column (Pavich et al., 1984), the total meteoric ^{10}Be in a minimally eroded terrestrial surface of known age can be used to estimate its average deposition rate over the soil's age (Reusser et al., 2010).

The present study aims to find the meteoric ^{10}Be flux from surface soils sample and tries to investigate its relation with amount of rainfall received in those regions.

2. MATERIALS AND METHODS

2.1 Sampling Location

To investigate the relationship between the flux of meteoric ^{10}Be from the atmosphere to the surface and regional rainfall levels, it is essential to select sampling locations that experience varying amounts of precipitation.. A good candidate as a place, fulfilling this necessary criterion is the Palghat/Palakkad Gap region in South India.

The Western Ghats form a continuous chain of hill peaks along the western escarpment of Indian Peninsula, extending from 8°N to 21°N latitude. Spanning approximately 1,490 km parallel to the west coast, this range is interrupted at 11°N by the 30 km wide Palghat Gap (Karuppusamy, 2024).

The Palghat Gap is a 30 km wide break in the Western Ghats, bordered by the Nilgiris to the north, with elevations ranging from approximately 1 to 1.5 km, and the Anamalai Hills to the south, rising between 2 and 2.5 km. In contrast, The Palghat Gap has an average elevation of approximately 200 m and is believed to have formed around 0.5 billion years ago. (Santosh et al., 1992; Soman et al., 1990). The gap is identified as a dextral shear zone, with its origin attributed to the combined effects of shearing and erosion (D'Cruz et al., 2000).

Ramachandran (1972) analyzed variations in rainfall and wind speed across three different cross-sections: one located north of the gap, another spanning the gap itself, and a third positioned to the south of the gap. He observed that in the northern and southern cross-sections of the gap, rainfall increases up to approximately 60 km from the western coast before declining on the leeward side of the Ghats. In the gap section, rainfall is continuously decreasing from the coast, with a sudden drop in rainfall from Chittur (in Kerala) to Pollachi (in Tamil nadu) in the lee-side of the gap section. The distance between Chittur and Pollachi in the gap section is only 25 km, but the rainfall decreased from 337.8 mm to 100.8 mm

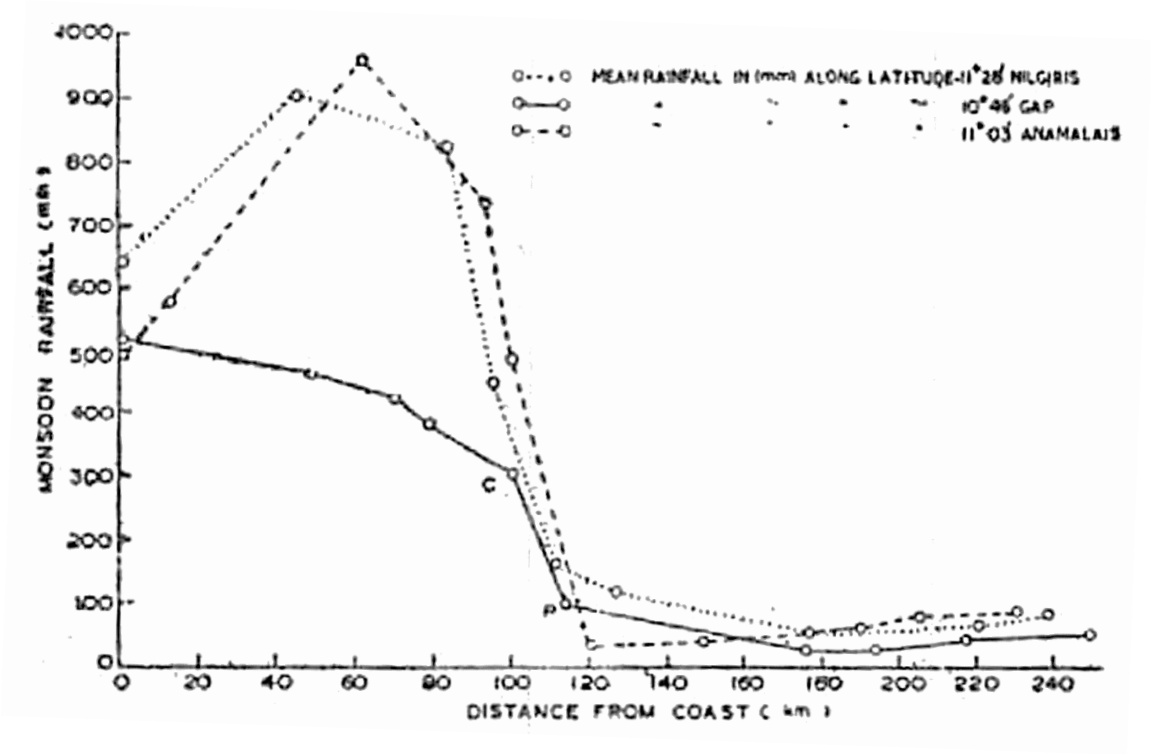

Figure 2.1: The mean SW monsoon rainfall during June- September plotted for three sections: continuous line – Across the gap, dotted line – along the northern flanks of the gap and dashed line – Across the southern flank of the gap. C and P corresponds to Chittur and Pollachi, respectively (Ramachandran,1972).

The rainfall data for this region, used in this study, was sourced from the India Meteorological Department (IMD) website (Pai et al., 2014).The yearly gridded rainfall (0.25 x 0.25) data for the years 2019 to 2023 was extracted and the average annual rainfall was calculated for the grids along the Palghat Gap. To the western side of the Western Ghat, that is in the Kerala region, the average annual rainfall is >2500 mm, which reduces to 1200 mm in the eastern side of the Gap. The rainfall then succumbs down to ~600 mm in the interior, Tamil Nadu region. Upon further study, it was also observed the rainfall amount further increased to 1600 mm towards the eastern ghat region. So, in the big picture, we have this really nice rainfall gradient zone in South India with a rainfall of >2600 mm in the western side, which halves down to 1200 mm and then further decrease to 600 mm as we move to the mainland Tamil Nadu, but also increases to 1600 mm further east.

A total of 15 grids with different annual rainfall amounts were identified for sampling and surface soil samples were taken from 16 different locations, with two different samples in the same grid, along this ‘corridor’. Since all of them are within the same latitude, the production of meteoric ^{10}Be would be same in all these locations. Any change in the production rate or any change in any of the large-scale atmospheric processes would affect all of the locations. So, one can arrive at a conclusion that any variation in the meteoric ^{10}Be inventory of the soils in these locations would reflect the changes in the depositional process and in the geochemistry of the soils.

Figure 2.2: Locations from where the sample was collected

There are some prerequisites which has to be met for determining site-specific ^{10}Be flux using dated soil profiles. There should be complete retention of meteoric ^{10}Be since the stabilization of the landform and prior to its stabilization, there must be negligible ^{10}Be inherited as they can lead to overestimation of ^{10}Be inventory. The surface erosion must also not lead to removal of Be isotopes (Deng et al., 2021). So, the locations should be chosen such that they have no slope sides and no extensive erosion (by flooding, high overland flow, strong windy areas etc.). The chosen profiles should also have neutral-high soil pH so that the desorption and remobilization of ^{10}Be might not occur. The sampling depth has also to be sufficient enough for quantification of inheritance (Deng et al., 2020). With this knowledge, the sampling was done. The samples were taken using a stainless-steel corer. Ideal location for such sampling would be the reserved forests. But there were no such forest regions in Tamil Nadu and it was sufficed by collecting the samples from seemingly undisturbed regions. Only once the sampling started in Kerala, it was possible to find such forest regions. So out of the 16 samples collected, 3 were

from forest areas. Also, all the samplings were done at low altitudes with an average of 131 m.

Figure 2.3: Sampling site (left) and the corer used for sampling (right)

2.2 Procedure

The general procedure for the measurement of the $^{10}Be/^{9}Be$ in almost all of the cosmogenic radionuclide laboratory in the world is depicted below.

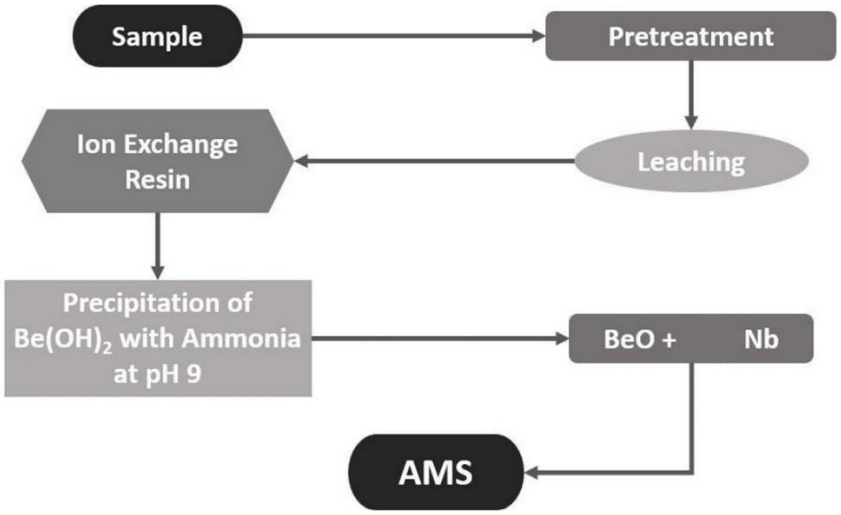

Figure 2.4: General procedure for both meteoric and '*in-situ*' ^{10}Be

In this study, the complete procedure for the extraction and measurement of ^{10}Be was according to the protocol established in Physical Research Laboratory (PRL), Ahmedabad for the work Jena et al., (2021) (Fig 2.5) and is explained below. The difference between the chemical procedure for meteoric and '*in-situ'* 10Be is that for *in-situ* the digestion is more extreme and quartz is extracted, which is then separated from other minerals and then dissolved using HF and then later by aqua-regia. The remaining steps of column chromatography and further steps are same for both the nuclides.

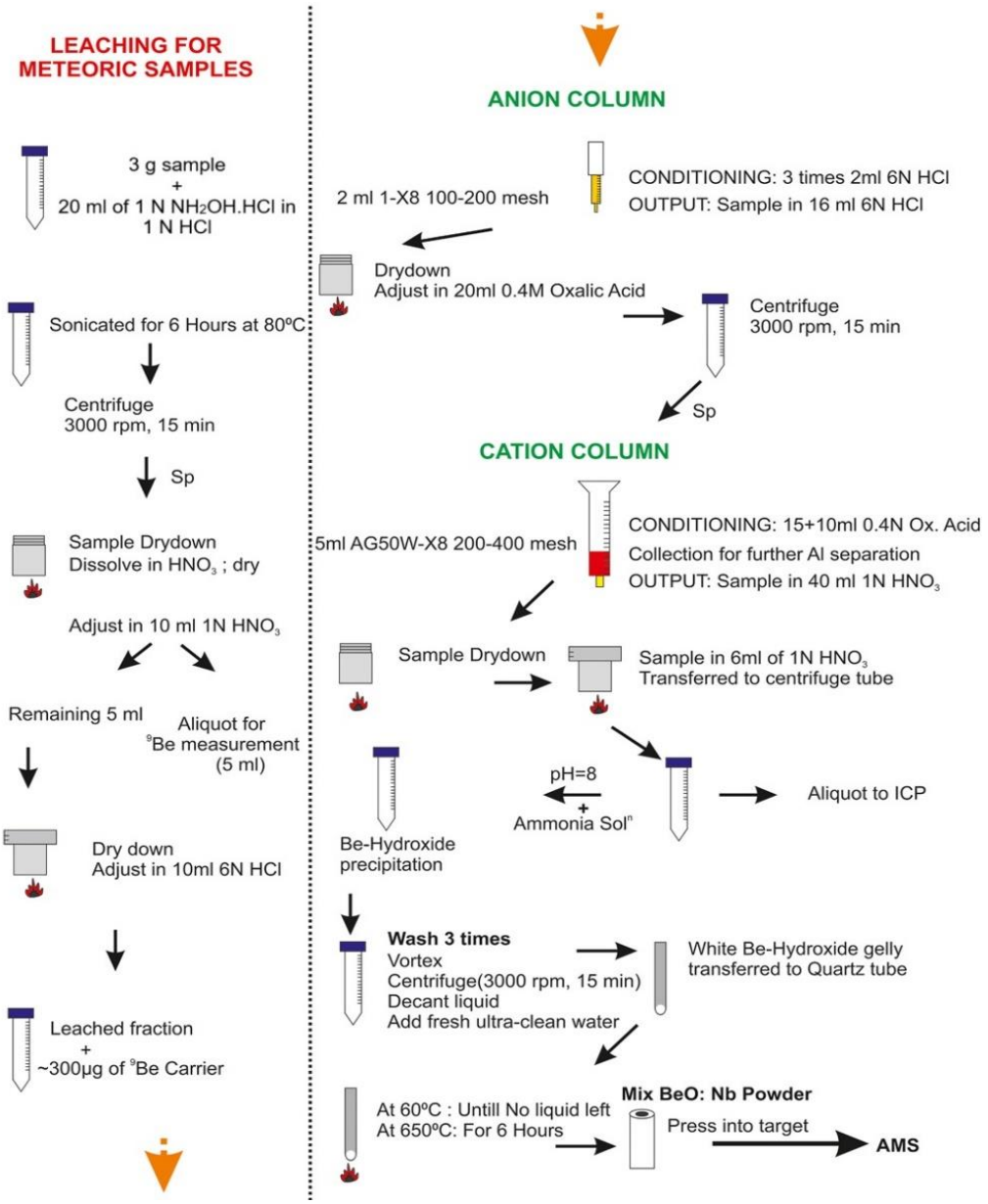

Figure 2.5: Complete procedure for meteoric ^{10}Be used in this work (Jena et al., 2021)

2.3 Meteoric ^{10}Be Procedure

2.3.1 ^{10}Be extraction

The surface soil samples were thoroughly mixed, air-dried and then crushed homogenously. 3 grams of sample were taken and then kept for leaching with 1 N hydroxylamine hydrochloride ($NH_2OH.HCl$) in 1 N HCl overnight. This a single-step extraction technique used for the extraction of beryllium isotopes, along with other elements. $NH_2OH.HCl$ is a powerful reducing agent and is capable of extracting the authigenic beryllium. They were then centrifuged the next day and the leachate is separated. Jena et al., (2021) had used a weak leaching agent, 0.04 M $NH_2OH.HCl$ in 25% acetic acid. Though, the efficiency of the extraction of Be isotopes from the reactive phase varies with different leaching procedures, the ^{10}Be/^{9}Be ratio appears to remain the same (Jeromson et al., 2021)

Figure 2.5.1: Samples kept for leaching

The leachate solution is dried and further digested with concentrated HNO_3 before being dissolved in 10 ml of 0.1 N HNO. Half of this solution (5 ml) is then taken for ^{9}Be measurement in Inductively Coupled Plasma Optical Emission Spectrometer, (ICP-OES) and the remaining half is further processed for ^{10}Be measurement. The latter is then dried and dissolved in 6 N HCl and is ready for the next step, which is the separation of Be from other elements using column chromatography.

Figure 2.5.2: Samples kept for drying in Teflon vials

2.3.2 ^{10}Be separation and purification

Prior to column chromatography, about 300 µl of Be carrier is added to the samples. This step is necessary because AMS requires high currents of the stable isotope, and since the natural abundance of ^{9}Be in samples is very low, the carrier is added to ensure sufficient ^{9}Be for accurate measurement (Romero et al., 2023).

The ^{10}Be which is now made available is then separated using two distinct ion exchange resins. The solution along with the carrier is first made to pass through an anion exchange resin. The resin used is 1-X8 100-200 mesh resin, which is a gel type resin or microporous resin. They are prepared from styrene, with 8% of the crosslinking agent divnyl benzene (PS-DVB resin). It is a Type 1 strong basic anion exchanger with the quaternary amine functional group, trimethyl ammonium, available in its chloride form ($R\text{-}CH_2N^+(CH_3)_3Cl^-$; R=PS-DVB copolymer). 2 ml of this resin is filled in 5 ml Biorad Poly-Prep® column and is then conditioned with 6 N HCl.

After passing the solution, iron is removed, which is indicated by the color transition of the solution from yellow to colourless. It is one of the few steps of the procedure where one can actually observe some changes.

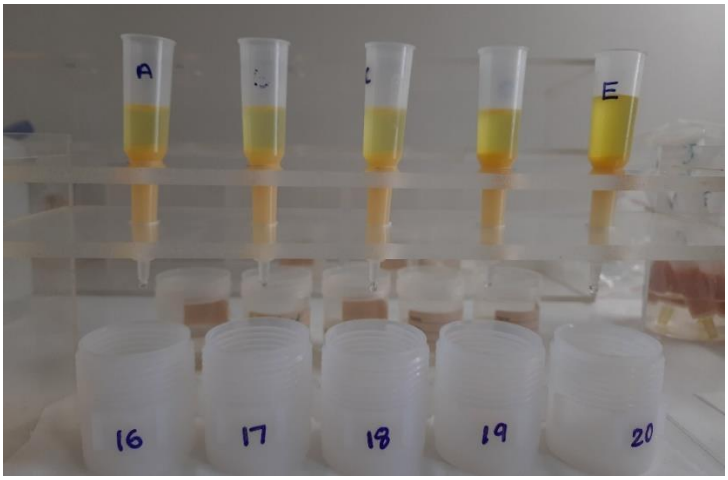

Figure 2.5.3: 5 ml Biorad Poly-Prep® column containing 2 ml of 1-X8 100-200 mesh resin

The sample is then dried and the solution medium is changed into 0.4 N oxalic acid. This precipitates out Ca as calcium oxalates, which are removed by centrifugation and the supernatant is then passed through a cation exchange resin. The resin used is the AG 50W-X8 200-400 mesh resin, which is a strongly acidic gel type cation exchanger with sulfonic acid functional group attached to the PS-DVB matrix ($R\text{-}SO_3^-H^+$). 5 ml of this resin is filled in 15 ml Biorad Econo-Pac® column and is then cleaned and conditioned with 5 N HNO_3 and 0.4 N oxalic acid,respectively. The end result after passing through this column is the separation Be from aluminium and sodium. It is noteworthy to mention that Al can also separated from this, which can be collected and used for its analysis.

Figure 2.5.3: 15 ml Biorad Econo-Pac® column containing 5 ml of AG 50W-X8 200-400 mesh resin

The sample, after drying again, is dissolved in 0.5 M HNO_3. The beryllium in it is precipitated by adding ammonia solution. The $Be(OH)_2$ precipitate can be seen as a thin, scanty transparent film or gel. This precipitate is cleaned further with ultrapure water to remove $B(OH)_3$ as it is soluble in water.

The final $Be(OH)_2$ precipitate is taken carefully using a pipette and shifted to a quartz tube, which is then kept in the oven for 60º C until it dries completely. They are then calcined in the furnace at 600º C for 6 hours for its conversion to BeO. It is this BeO which is used for measuring the $^{10}Be/^{9}Be$ ratio. The BeO is combined with Nb powder, which functions as a thermoelectric conductor to facilitate the generation of negative ions (Romero et al., 2023), ultimately improving the beam current within the AMS. This BeO-Nb mixture is then compacted into aluminum cathodes and subsequently positioned in the AMS for measuring the beryllium isotopic ratio.

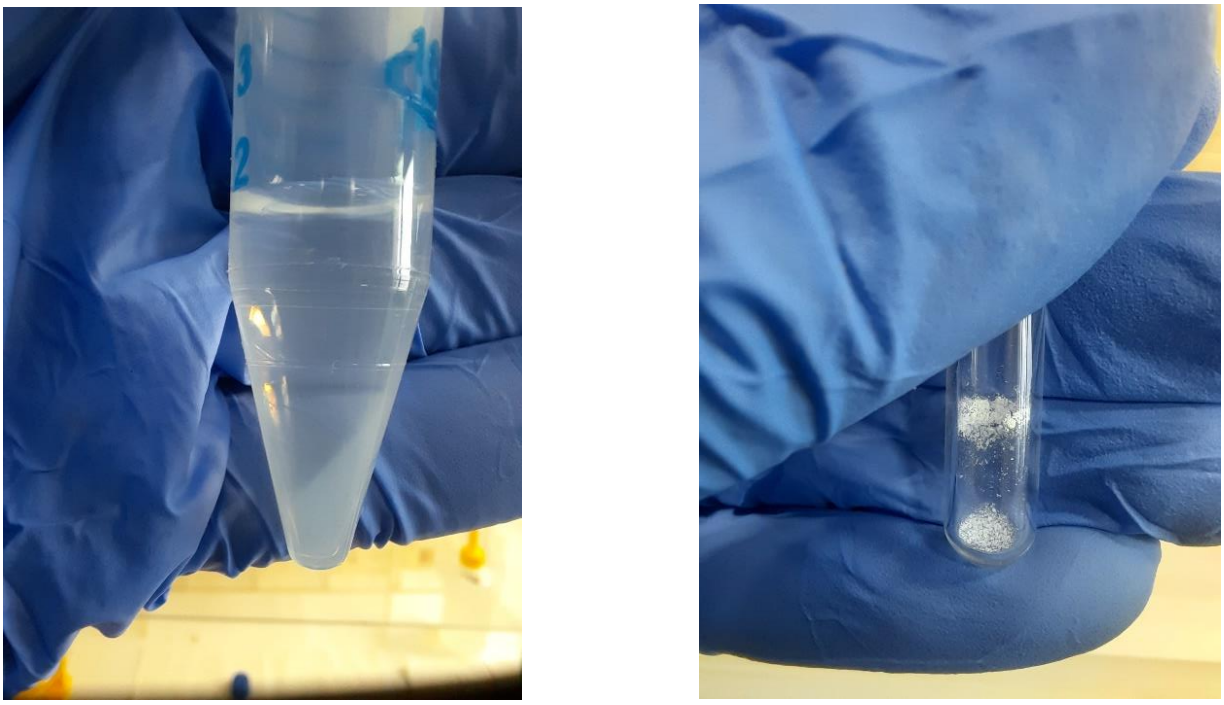

Figure 2.5.4: $Be(OH)_2$ at the bottom of the centrifuge tube seen as a thin film of precipitate, (left) which is converted to BeO powder (right)

2.3.3 ^{10}Be Isotopic measurement

The $^{10}Be/^{9}Be$ ratio is determined in Accelerator Mass Spectrometer (AMS), which combines particle accelerator techniques into a mass spectrometer. Initially developed for measuring the $^{14}C/C$ ratios, they have been extended to the measurement of other isotopic ratios like ^{10}Be, ^{26}Al, ^{36}Cl etc. Accelerator mass spectrometry integrates the high efficiency of mass spectrometry with superior capability to distinguish isobaric, isotopic, and molecular interferences (Fifield.,2005) and is designed to count single atoms of one very rare isotope, like the cosmogenic nuclides, in the presence of the stable isotopes with up to 10^{15} or even 10^{16} times higher abundances. This exceptional sensitivity revolutionized cosmogenic nuclide techniques and has been used for their analysis ever since.

For this study, the beryllium isotopic ratio was measured using the Accelerator Unit for Radio-isotope Studies (PRL-AURiS) (Bhushan et al., 2018), a 1MV AMS system acquired from High Voltage Engineering Europa, BV, Netherlands (Klein et al., 2006).

PRL-AURiS consists of multiple components - negative ion source, a low-energy (LE) bouncer injector magnet, a 1 MV tandetron accelerator, a high-energy (HE) magnet, a 150 nm silicon nitride (SiN) foil, an electrostatic analyzer (ESA), a rare isotope (RI) magnet, and a gas ionization chamber (GIC) detector (Bhushan et al., 2018; Jena,2022).

Figure 2.6: 1 MV AMS at PRL, Ahmedabad

In the ion source, negative ions are produced by a process called sputtering. Cesium is present in the reservoir which is heated at 110ºC produce its vapours. These Cs vapours are positively ionized by an ionizer and when a target voltage is applied between the target (sample in the cathode) and the ionizer, the positive Cs ions strike the target and they induce the release of negative ions through sputtering. These negative sample ions are then accelerated by the target voltage toward the ionizer.

The ion beam is directed through a low-energy magnet, referred to as the Bouncer-Injector magnet. By applying different DC voltage pulses between the ion source (at ground potential) and the magnet's electrically insulated vacuum chamber, stable and rare isotopes of interest are sequentially selected—a process known as bouncing. As the ions enter the magnet chamber, they undergo acceleration, while upon exiting, they experience deceleration. This results in the two isotopes acquiring different energy levels as they traverse the constant magnetic field. The production of ions of the stable isotope are several orders high compared to the rare isotope, leading to different electrical load in the accelerator tube and further leading to variations in the voltage (Hellborg and Skog, 2008). Consequently, stable isotopes are injected into the accelerator for a shorter duration than rare isotopes (Bhushan et al., 2018). Once injected into the accelerator, the negative ions undergo a stripping process, where argon gas breaks the molecules, generating positive ions of the element. This process significantly increases the ion beam energy, aiding in their identification in the final detector.

Following acceleration, the high-energy magnet analyzes the beam of positive ions, separating stable isotopes based on their distinct curvature radii. These isotopes are then collected in an off-set Faraday cup (or cups, in the case of carbon, for separating ^{12}C and ^{13}C, from ^{14}C). The rare isotope beam then travels through an Electrostatic Analyzer and a Rare Isotope magnet, which filter out unwanted ions and minimize the measurement background. Finally, the final residual energy (E_{res} or E_{final}) and energy loss (ΔE) of the rare isotope are measured by the gas-filled dual-anode ionization chamber detector. This enables the differentiation of unwanted ions based on their distinct energy loss characteristics.

In case of Be, it does not form a stable atomic negative ion (Fifield, 2005). Hence this is the reason why the samples are prepared as BeO. Both $^{9}BeO^{-}$ and $^{10}BeO^{-}$ are injected into the accelerator, where by the stripping process, these negative molecular ions are broken into positive Be ions, which are then passed through the HE magnet to separate it from the stable isotopic ion.

Boron-10 is the stable isobar of ^{10}Be and readily forms BO^{-}, allowing it to travel alongside ^{10}Be after acceleration. To separate them, a 75 nm thick silicon nitride foil is placed in its path before the electrostatic analyzer. The foil creates a difference in the residual energy of transmitted ^{10}B and ^{10}Be, as B ions decelerate more quickly than Be ions. This energy variation enables the Electrostatic Analyzer (ESA) to distinguish between the two ions. Finally in the detector, beryllium is separated from the boron and other interferences in the E_{res} and ΔE plot.

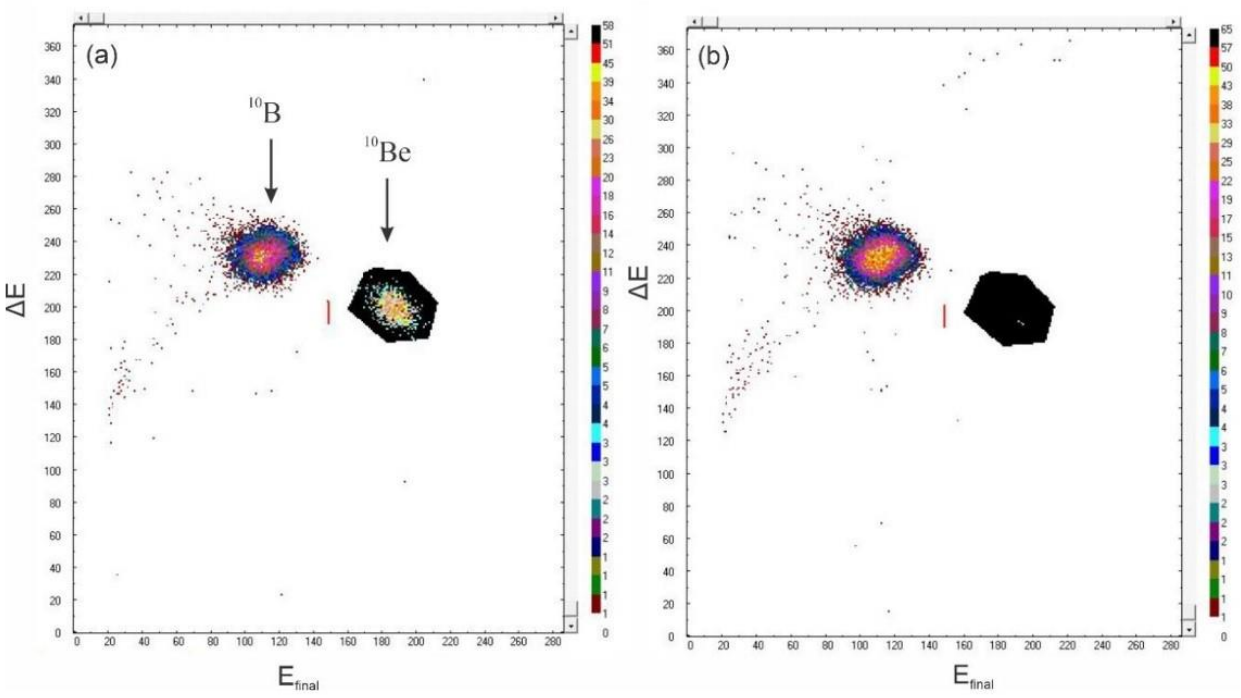

Figure 2.7: Typical ΔE vs. E_{final} plot for Be isotopes measured with AMS, for (a) a sample and (b) a blank. The black polygon marks the selected Region of Interest (ROI) for ^{10}Be counting (Jena, 2022)

The concentration of ^{9}Be is measured in Thermo Scientific iCAP 7000 Plus series Inductively Coupled Plasma Optical Emission Spectrometer (ICP-OES) at PRL (Jena,2022). It consists of a sample injection system, plasma torch, radiofrequency power generator, an echelle optical design, and a charge injection device (CID) solid-state detector.

The instrument processes liquid samples, which are pumped through a nebulizer to generate a fine spray. These fine aerosols are then directed into the plasma, where high temperatures break them down into atoms and ions. Within the plasma chamber, the atoms are excited by the electrical Radio Frequency generated plasma. As these excited atoms return to their ground state, they emit characteristic wavelengths unique to each element. The intensity of the emitted wavelength is then measured, corresponding to the sample's concentration

Figure 2.8: ICP-OES at PRL, Ahmedabad

The optical system of the ICP-OES includes an echelle grating and a prism. Their typical alignment produces a two-dimensional spectrum, known as an 'echellegram,' which enables wavelength and order separation. The instrument can measure wavelengths ranging from 166 to 847 nm.

3. RESULTS AND DISCUSSIONS

3.1 Results

The samples were run in batches of five, with each batch containing 1 full process blank and 4 samples. To compensate for Be present in the carrier and any introduced during sample processing, the blank $^{10}Be/^{9}Be$ ratio is directly subtracted from the measured sample ratios. Because both ^{10}Be and ^{9}Be are measured in different detectors, in addition to a longer travel path for ^{10}Be and an additional loss of ^{10}Be in the SiN foil, the blank corrected $^{10}Be/^{9}Be$ ratio of the sample has to be normalized with a standard whose $^{10}Be/^{9}Be$ ratio is known. The ^{10}Be-14-5-6 standard with a $^{10}Be/^{9}Be$ ratio of 1.504×10^{-11} (Nishiizumi, 2022; Nishiizumi et al., 2007) was used for normalization.

$$\left(^{10}Be/\,^{9}Be\right)_{AMS} = \{\left(^{10}Be/\,^{9}Be\right)_{Raw} - \left(^{10}Be/\,^{9}Be\right)_{Blank}\} \times \frac{\left(^{10}Be/\,^{9}Be\right)_{Standard,known}}{\left(^{10}Be/\,^{9}Be\right)_{Standard,measured}}$$

Equation 3.1: Equation for finding the $(^{10}Be/^{9}Be)_{AMS}$ from AMS raw data

The calculation of the real $^{10}Be/^{9}Be$ of the sample requires calculating the ^{10}Be and ^{9}Be atoms per gram of the soil. This is obtained by the following formula (Jena et al., 2022).

$$^{9}Be\ (atoms\ g^{-1}) = f_9 \times \frac{[Be] \times N_A \times V_{half}}{M_{Be} \times 10^9} / W_{soil}$$

$$^{10}Be\ (atoms\ g^{-1}) = f_{10} \times \left(\frac{^{10}Be}{^{9}Be}\right)_{AMS} \times \left(\frac{[Be] \times N_A \times V_{half}}{M_{Be} \times 10^9} + \frac{W_c \times N_A}{M_{Be} \times 10^6}\right) / W_{soil}$$

Equation 3.2: Equation to find the ^{10}Be and ^{9}Be concentration in the sample where f_9 and f_{10} are dilution factors, defined as the ratio of the total leach solution volume (10 ml) to the volume taken for analysis (V_{half}, = 5 ml for both ^{9}Be and ^{10}Be), which results in a value of 2 in this study. $[Be]$ is the beryllium concentration from ICP-OES (in ppb), N_A is the Avogadro's constant and M_{Be} is the atomic mass of beryllium. W_{soil} is the sample amount taken for leaching and W_c weight of the carrier added.

Dividing these two gives the $^{10}Be/^{9}Be$ of the sample

$$\left(\frac{^{10}Be}{^{9}Be}\right)_{AMS} = \frac{^{10}Be\ (atoms\ g^{-1})}{^{9}Be\ (atoms\ g^{-1})}$$

Equation 3.3: Equation for finding the $^{10}Be/^{9}Be$ of the sample

The ^{10}Be concentration in the samples varies from $15.0*10^{7}$ atoms/gram to $1.54*10^{7}$ atoms/ gram, which corresponds to sites receiving an average rainfall of 639.9 mm/year and 608.8 mm/year respectively. While the site receiving the lowest rainfall amount of 608.8 mm has the lowest meteoric ^{10}Be concentration of $1.54*10^{7}$ atoms/gram, which is as expected, the site receiving the largest rainfall of 2859 mm has a meteoric ^{10}Be concentration of $7.28*10^{7}$ atoms/gram, which is half the concentration of the highest value.

The $^{10}Be/^{9}Be$ ratio is different from this pattern with a highest value of $4.77*10^{-9}$ and a lowest value of $1.18*10^{-9}$ at sites receiving average annual rainfall of 814.3 mm and 1974.2 mm, respectively.

Assuming there is no inheritance of meteoric ^{10}Be from other sources to sample location, its inventories at the surface I(atoms/cm^2) can be calculated by following (Ouimet et al., 2015):

$$I = [Be] \times \rho_s \times h$$

Equation 3.4: Equation to calculate the meteoric ^{10}Be inventories where $[Be]$ is ^{10}Be concentration (atoms/ g), ρ_s is bulk density (g/ cm^3), and h is thickness (cm).

The ^{10}Be inventories varies from $1.00*10^{8}$ to $9.78*10^{8}$ atoms/cm^2. The site receiving the lowest rainfall amount of 608.8 mm has the lowest meteoric ^{10}Be inventory of $1.00*10^{8}$ atoms/cm^2 and the site receiving the largest rainfall of 2859 mm has a meteoric ^{10}Be concentration of $9.78*10^{8}$ atoms/cm^2.

Most soils retain all of the deposited meteoric ^{10}Be within the soil column (Pavich et al., 1984). Hence, for a minimally eroded terrestrial surface (of known age), its total meteoric ^{10}Be can be used to calculate its average deposition rate over the age of the soil (Reusser et al., 2010).

Considering there is no decay of this deposited ^{10}Be over the soil formation time t (years), the flux of the meteoric ^{10}Be, F (atoms/cm^2/year) can found by:

$$F = {}^{I}/_{t}$$

Equation 3.5: Equation to fond the depositional flux

For the entire duration of the formation of the top few centimeters of soil which were used for this study, which is approximately 300 years, the flux values range from 0.32*10^6 to 3.13*10^6 atoms/cm^2/year. The region receiving the highest rainfall of 2859 mm had a flux of 1.51*10^6 atoms/cm^2/year, which is about half of the highest flux value. The site having the lowest rainfall had the lowest flux value of 0.32*10^6 atoms/cm^2/year. Contrary to the assumption of flux values being proportional to rainfall received, the present study shows a different relationship between the two. The flux value increases linearly with rainfall for regions receiving rainfall <1500 mm/year and it decreases with increasing rainfall in places having an annual rainfall > 1500 mm/year.

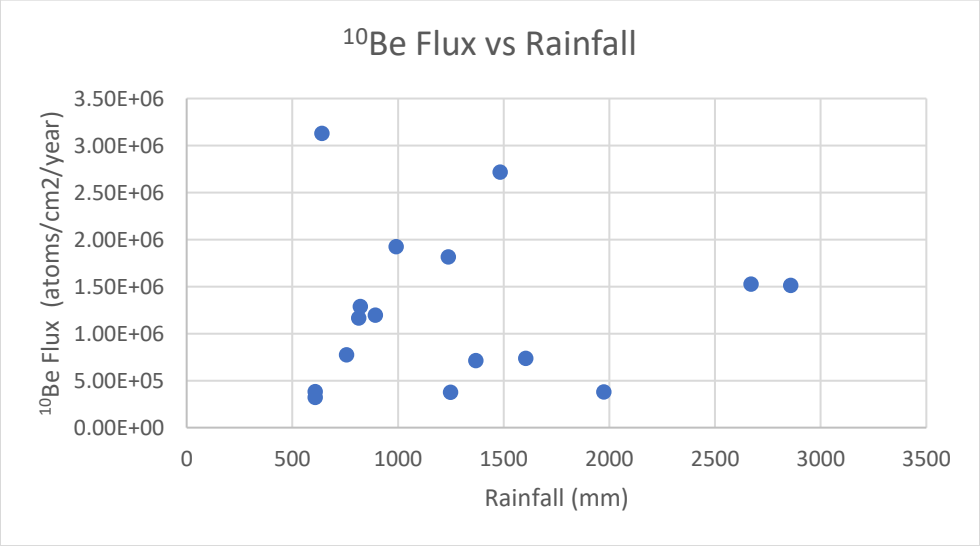

Figure 3.1: Meteoric ^{10}Be flux plotted against annual average precipitation rates

Out of the 16 samples, two of them were taken from the same grid receiving an annual rainfall of 608 mm. Though they were taken from different locations within the same grid, they have similar flux values of $0.32*10^6$ atoms/cm^2/year and $0.38*10^6$ atoms/cm^2/year.

3.2 Discussion

The obtained meteoric ^{10}Be concentrations in the soil samples show good agreement with previously reported studies. Dixon et al., (2018) had measured the meteoric ^{10}Be in the soils of the lava flows of Hawaii, along sites receiving 160-3000 mm of annual rainfall. He observed that ^{10}Be concentration increase linearly with rainfall but upto 1400 mm annual rainfall, beyond which its concentration decreases. Similar result was also obtained by Chen et al., (2020) from soils measured in China. The study showed that in low-precipitation regions (< 1200 mm/y), the soil meteoric ^{10}Be concentration increases with rainfall, but in high-precipitation regions (> 1200 mm/y) its concentration showed negative correlation with precipitation. The present study also has a threshold of precipitation beyond which both the ^{10}Be concentration and the flux values are low with further increase in precipitation.

There can be mainly two possible reasons for such a pattern. One is the loss of ^{10}Be from regions of high rainfall while the other is the additional gain of ^{10}Be in regions of low rainfall. In the case of the former, one more player comes into the picture – the retention of ^{10}Be to the soil. The retention of ^{10}Be depends on the geochemistry of the soils. For very low pH, beryllium is soluble. Laboratory experiments conducted by Boschi and Willenbring (2016a) demonstrated that increasing the pH from 4 to 6 resulted in a 79–2270% higher retention of Be by various organic compounds and minerals. Desorption experiments by Boschi and Willenbring (2016b) revealed that lowering pH caused the greatest desorption of Be from clay minerals. However, no such desorption was observed in the case of organic ligands. Instead, a decrease in pH led to an increase in beryllium sorption. This suggests that even at low pH, where beryllium is released from minerals, its complexation with organic molecules helps retain it in the soil, preventing loss.

Thus, soil geochemistry actively minimizes beryllium loss under all conditions, ensuring the retention of deposited ^{10}Be. But in spite of this, a sufficiently high water throughput can result in the loss or translocation of beryllium within the soil (Singleton, 2021). Dixon et al. (2018) observed that across Hawaii's rainfall gradient, ^{10}Be inventories decrease as the water balance turns positive. This reduction is linked to increased water movement through the soil column, marking the threshold for Be mobility and desorption in the upper soil horizons where ^{10}Be is deposited. Chen et al. (2020) concluded that frequent heavy rainfall in high-precipitation regions facilitates the transfer of ^{10}Be to fluvial systems before it can securely bind to the soil. Both findings highlight runoff as a key factor explaining the similar ^{10}Be concentration patterns observed in this study.

Strong winds can relocate ^{10}Be from its initial deposition site to other regions by transporting it as dust (Lal, 2007; Willenbring and von Blanckenburg, 2010). There is a possibility of the southwest monsoon winds carrying the dust containing ^{10}Be from the high precipitation region of Kerala, resulting in a lower ^{10}Be inventory in this region, to the interior part of Tamil Nadu along its path and loading them in this region, leading to an anomalously high ^{10}Be inventory of $9.78*10^8$ atoms/cm^2 at sample location 6. But these dust-derived ^{10}Be fluxes are orders of magnitude smaller than atmospheric deposition and are not regarded as a major source of uncertainty (Willenbring and von Blanckenburg, 2010).

The existing pattern of ^{10}Be flux could also be due to the interplay of the two delivery effects: dilution and additive effect. In an additive effect, both water vapor and ^{10}Be are continuously supplied to advective clouds during their long transport, resulting in increasing ^{10}Be fluxes with higher precipitation levels. The concentration of ^{10}Be in precipitation can be reduced due to the dilution effect, which occurs during convective precipitation, where clouds have high turnover rates and vapor sources are close to the rainfall location. In this case, the flux of ^{10}Be is limited by the rate at which it is introduced into the clouds after its production (Willenbring and von Blanckenburg, 2010). In this scenario, while the ^{10}Be flux remains constant, its concentration varies depending on the extent of dilution by water vapor.

The interplay of all these factors results in the following flux values of meteoric ^{10}Be across the Palghat Gap. Though not quantitatively, the flux of ^{10}Be almost qualitatively reflects the rainfall pattern observed in this region.

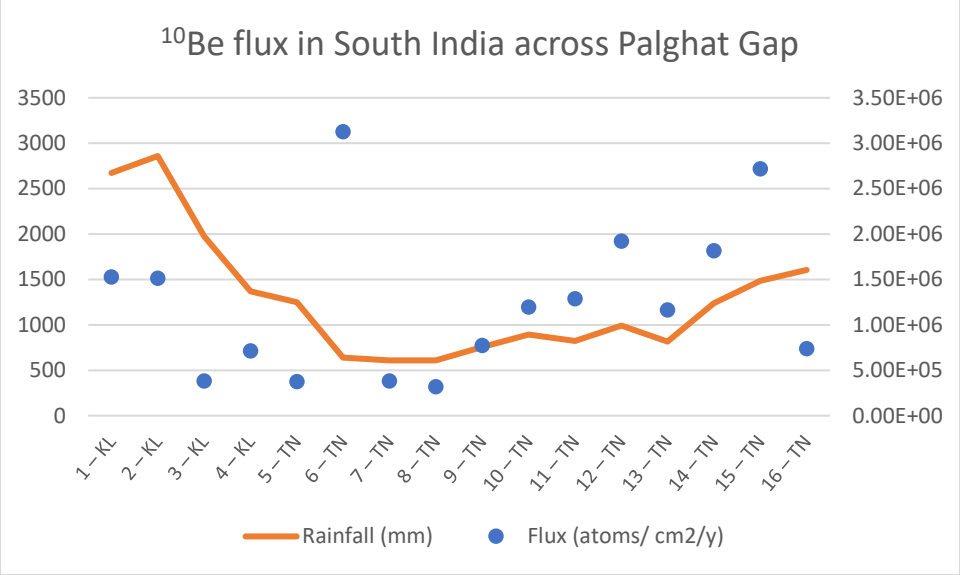

Figure 3.2: Flux of meteoric ^{10}Be measured from soil samples along the Palghat Gap from West (Kerala; depicted as KL) to east (Tamil Nadu; depicted as TN)

Therefore, in a given region, higher precipitation does not necessarily correspond to increased ^{10}Be deposition, but lower precipitation always leads to reduced ^{10}Be reaching the surface.

REFERENCES

1. Baade, W., & Zwicky, F. (1934). Cosmic rays from super-novae. Proceedings of the National Academy of Sciences, 20(5), 259-263.
2. Beer, J., McCracken, K., & Steiger, R. (2012). Cosmogenic radionuclides: theory and applications in the terrestrial and space environments. Springer Science & Business Media.
3. Bhushan, R., Yadava, M. G., Shah, M. S., & Raj, H. (2019). Performance of a new 1MV AMS facility (AURiS) at PRL, Ahmedabad, India. Nuclear Instruments and Methods in Physics Research Section B: Beam Interactions with Materials and Atoms, 439, 76-79.
4. Boschi, V., & Willenbring, J. K. (2016a). The effect of pH, organic ligand chemistry and mineralogy on the sorption of beryllium over time. *Environmental Chemistry*, *13*(4), 711-722.
5. Boschi, V., & Willenbring, J. K. (2016b). Beryllium desorption from minerals and organic ligands over time. *Chemical Geology*, *439*, 52-58.
6. Bourcier, L., Masson, O., Laj, P., Chausse, P., Pichon, J. M., Paulat, P., ... & Sellegri, K. (2012). A new method for assessing the aerosol to rain chemical composition relationships. Atmospheric research, 118, 295-303.
7. Chen, P., Yi, P., Czymzik, M., Aldahan, A., Ljung, K., Yu, Z., ... & Possnert, G. (2020). Relationship between precipitation and 10Be and impacts on soil dynamics. Catena, 195, 104748.
8. D'Cruz E, Nair PKR, Prasannakumar V (2000) Palghat Gap—A Dextral Shear Zone from the South Indian Granulite Terrain. Gondwana Res 3(1):21–31.
9. Deng, K., Wittmann, H., & von Blanckenburg, F. (2020). The depositional flux of meteoric cosmogenic 10Be from modeling and observation. Earth and Planetary Science Letters, 550, 116530.
10. Deng, K., Wittmann, H., Hsieh, M. L., Yang, S., & von Blanckenburg, F. (2021). Deposition and retention of meteoric 10Be in Holocene Taiwan river terraces. Quaternary Science Reviews, 265, 107048.

11. Dixon, J. L., Chadwick, O. A., & Pavich, M. J. (2018). Climatically controlled delivery and retention of meteoric 10Be in soils. Geology, 46(10), 899-902.
12. Dunai, T. J. (2010). Cosmogenic nuclides: principles, concepts and applications in the earth surface sciences. Cambridge University Press.
13. Fifield, L. K. (2005). Accelerator mass spectrometry. In Electrostatic Accelerators: Fundamentals and Applications (pp. 461-485). Berlin, Heidelberg: Springer Berlin Heidelberg.
14. Grieder, P. K. (Ed.). (2001). Cosmic rays at Earth. Elsevier.
15. Golubenko, K. (2023). Cosmogenic isotopes produced by galactic cosmic rays and extreme solar events in the Earth's atmosphere.
16. Goswami, J. N., & Macdougall, J. D. (2021). Devendra Lal. 14 February 1929—1 December 2012.
17. Graly, J. A., Reusser, L. J., & Bierman, P. R. (2011). Short and long-term delivery rates of meteoric 10Be to terrestrial soils. Earth and Planetary Science Letters, 302(3-4), 329-336.
18. Heikkilä, U., Beer, J., & Feichter, J. (2009). Meridional transport and deposition of atmospheric 10 Be. Atmospheric Chemistry and Physics, 9(2), 515-527.
19. Heikkilä, U., Heikkilä, U., Beer, J., Abreu, J.A., & Steinhilber, F. (2013). On the Atmospheric Transport and Deposition of the Cosmogenic Radionuclides (10Be): A Review. Space Science Reviews, 176, 321-332.
20. Hellborg, R., & Skog, G. (2008). Accelerator mass spectrometry. Mass spectrometry reviews, 27(5), 398-427.
21. Ishikawa, Y., Murakami, H., Sekine, T., & Yoshihara, K. (1995). Precipitation scavenging studies of radionuclides in air using cosmogenic 7Be. Journal of Environmental Radioactivity, 26(1), 19-36.
22. Jena, P. S., Bhushan, R., Shivam, A., Nambiar, R., & Bharti, N. (2021). Production rate variation and changes in sedimentation rate of marine core dated with meteoric 10Be and 14C. Journal of Environmental Radioactivity, 237, 106678.
23. Jena, P. S. (2022). Applications of cosmogenic nuclides in understanding Quaternary events (Doctoral dissertation, PhD Thesis). Indian Institute of Technology Gandhinagar).

24. Jena, P. S., Bhushan, R., Ajay, S., Bharti, N., & Sudheer, A. K. (2022). 10Be depositional flux variation in the central Indian Ocean during the last 43 ka. Science of the Total Environment, 802, 149808.
25. Jeromson, M. R., Fujioka, T., Fink, D., Post, A. L., Simon, K. J., Sánchez-Palacios, J. T., ... & White, D. A. (2021). Extracting 10Be and 9Be from Antarctic marine sediments–a comparison of different extraction techniques.
26. Junge, C. E., & Junge, C. E. (1963). Air chemistry and radioactivity (Vol. 382, p. 1963). New York: academic press.
27. Karuppusamy, S. (2024). Physiography and Climatology of the Western Ghats. In Biodiversity Hotspot of the Western Ghats and Sri Lanka (pp. 5-23). Apple Academic Press.
28. Kaste, J. M., & Baskaran, M. (2012). Meteoric 7 Be and 10 Be as process tracers in the environment. Handbook of Environmental Isotope Geochemistry: Vol I, 61-85.
29. Klein, M. G., Mous, D. J. W., & Gottdang, A. (2006). A compact 1 MV multi-element AMS system. Nuclear Instruments and Methods in Physics Research Section B: Beam Interactions with Materials and Atoms, 249(1-2), 764-767.
30. Kulan, A. (2007). Atmospheric production and transport of cosmogenic 7Be and 10Be (Doctoral dissertation, Acta Universitatis Upsaliensis).
31. Laguionie, P., Roupsard, P., Maro, D., Solier, L., Rozet, M., Hébert, D., & Connan, O. (2014). Simultaneous quantification of the contributions of dry, washout and rainout deposition to the total deposition of particle-bound 7Be and 210Pb on an urban catchment area on a monthly scale. Journal of aerosol science, 77, 67-84.
32. Lal, D. (1991). Cosmic ray labeling of denudation surfaces: in situ nuclide production rates and denudation models. Earth and Planetary Science Letters, 104, 424-439.
33. Lal, D., & Peters, B. (1967). Cosmic ray produced radioactivity on the Earth. In Kosmische Strahlung II/cosmic rays II (pp. 551-612). Berlin, Heidelberg: Springer Berlin Heidelberg.

34. Lal, D., Malhotra, P. K., & Peters, B. (1958). On the production of radioisotopes in the atmosphere by cosmic radiation and their application to meteorology. Journal of Atmospheric and Terrestrial Physics, 12(4), 306-328.
35. Masarik, J., & Beer, J. (1999). Simulation of particle fluxes and cosmogenic nuclide production in the Earth's atmosphere. Journal of Geophysical Research: Atmospheres, 104(D10), 12099-12111.
36. Masarik, J., & Beer, J. (2009). An updated simulation of particle fluxes and cosmogenic nuclide production in the Earth's atmosphere. Journal of Geophysical Research: Atmospheres, 114(D11).
37. McHargue, L. R., & Damon, P. E. (1991). The global beryllium 10 cycle. Reviews of Geophysics, 29(2), 141-158.
38. Nishiizumi, K., Imamura, M., Caffee, M. W., Southon, J. R., Finkel, R. C., & McAninch, J. (2007). Absolute calibration of 10Be AMS standards. Nuclear Instruments and Methods in Physics Research Section B: Beam Interactions with Materials and Atoms, 258(2), 403-413.
39. Nishiizumi, K. (2022). Preparation of new 10Be and 26Al AMS standard reference materials. Nuclear Instruments and Methods in Physics Research Section B: Beam Interactions with Materials and Atoms, 530, 43-47.
40. Ouimet, W., Dethier, D., Bierman, P., Wyshnytzky, C., Shea, N., & Rood, D. H. (2015). Spatial and temporal variations in meteoric 10Be inventories and long-term deposition rates, Colorado Front Range. Quaternary Science Reviews, 109, 1-12.
41. Papastefanou, C. (2008). Radioactive aerosols. Radioactivity in the Environment, 12, 11-58.
42. Pai, D. S., Rajeevan, M., Sreejith, O. P., Mukhopadhyay, B., & Satbha, N. S. (2014). Development of a new high spatial resolution (0.25× 0.25) long period (1901-2010) daily gridded rainfall data set over India and its comparison with existing data sets over the region. Mausam, 65(1), 1-18.
43. Pavich, M. J., Brown, L., Klein, J., & Middleton, R. (1984). 10Be accumulation in a soil chronosequence. Earth and Planetary Science Letters, 68(2), 198-204.
44. Ramachandran, G. (1972). The role of orography on wind and rainfall distribution in and around a mountain gap: Observational study. MAUSAM, 23(1), 41-44

45. Reusser, L., Graly, J., Bierman, P., & Rood, D. (2010). Calibrating a long-term meteoric 10Be accumulation rate in soil. *Geophysical Research Letters*, *37*(19).
46. Rodhe, H., & Grandell, J. A. N. (1972). On the removal time of aerosol particles from the atmosphere by precipitation scavenging. *Tellus*, *24*(5), 442-454.
47. Romero, L. R., Ramírez-Martínez, C. J., Méndez-García, C. G., Padilla, S., Solís, C., & Huerta, H. (2023, October). Optimization of BeO formation parameters for the measurement of 10Be by AMS. In Journal of Physics: Conference Series (Vol. 2619, No. 1, p. 012017). IOP Publishing.
48. Santosh M, Kagami H, Yoshida M, Nanda-Kumar V (1992) Pan-African charnockite formation in East Gondwana: geochronologic (Sm-Ndand Rb-Sr) and petrogenetic constraints. Bull Indian Geol Assoc 25:1–10
49. Schaar, K., Spiegl, T., Langematz, U., Sato, T., Mekhaldi, F., Kunze, M., ... & Yoden, S. (2024). The role of deposition of cosmogenic 10Be for the detectability of solar proton events. *Journal of Geophysical Research: Atmospheres*, *129*(11), e2023JD040463.
50. Simpson, J. A. (1983). Elemental and isotopic composition of the galactic cosmic rays. *Ann. Rev. Nucl. Part. Sci.;(United States)*, *33*.
51. Singleton, A. (2021). *Terrestrial Archives of Meteoric 10BE* (Master's thesis, Purdue University).
52. Soman K, Thara KG, Arakelyants MM, Golubyev VN (1990) Mineral ages of pegmatites from the Palghat gap region in Kerala and their tectonic signifcance. J Geol Soc India 35:82–86
53. Usoskin IG, Solanki SK, Kovaltsov GA, Beer J, and Kromer B (2006) Solar proton events in cosmogenic isotope data. Geophysical Research Letters 33: L08107